



HAL
open science

Enhanced dielectric and electrocaloric properties in lead-free rod-like BCZT ceramics

Zouhair Hanani, Soukaina Merselmiz, Abdelaadim Danine, Nicolas Stein, Daoud Mezzane, M'barek Amjoud, Mohammed Lahcini, Yaovi Gagou, Matjaz Spreitzer, Damjan Vengust, et al.

► **To cite this version:**

Zouhair Hanani, Soukaina Merselmiz, Abdelaadim Danine, Nicolas Stein, Daoud Mezzane, et al.. Enhanced dielectric and electrocaloric properties in lead-free rod-like BCZT ceramics. *Journal of Advanced Ceramics*, 2020, 9 (2), pp.210-219. 10.1007/s40145-020-0361-1 . hal-02635246

HAL Id: hal-02635246

<https://hal.science/hal-02635246>

Submitted on 29 Jun 2020

HAL is a multi-disciplinary open access archive for the deposit and dissemination of scientific research documents, whether they are published or not. The documents may come from teaching and research institutions in France or abroad, or from public or private research centers.

L'archive ouverte pluridisciplinaire **HAL**, est destinée au dépôt et à la diffusion de documents scientifiques de niveau recherche, publiés ou non, émanant des établissements d'enseignement et de recherche français ou étrangers, des laboratoires publics ou privés.

Enhanced dielectric and electrocaloric properties in lead-free rod-like BCZT ceramics

Zouhair HANANI^{a,b}, Soukaina MERSELMIZ^a, Abdelaadim DANINE^c, Nicolas STEIN^c, Daoud MEZZANE^a, M'barek AMJOUD^{a,*}, Mohammed LAHCINI^{a,d}, Yaovi GAGOU^e, Matjaz SPREITZER^f, Damjan VENGUST^f, Zdravko KUTNJAK^f, Mimoun El MARSSI^e, Igor A. LUK'YANCHUK^{e,g}, Mohamed GOUNÉ^b

^aIMED-Lab, Cadi Ayyad University, Marrakesh 40000, Morocco

^bICMCB, University of Bordeaux, Pessac 33600, France

^cIJL, University of Lorraine, Nancy 54000, France

^dUM6P, Ben Guerir 43150, Morocco

^eLPMC, University of Picardy Jules Verne, Amiens 80039, France

^fJozef Stefan Institute, Ljubljana 1000, Slovenia

^gPhysics Faculty, Southern Federal University, Rostov-on-Don 344090, Russia

Received: October 29, 2019; Revised: December 24, 2019; Accepted: January 12, 2020

© The Author(s) 2020.

Abstract: Ba_{0.85}Ca_{0.15}Zr_{0.10}Ti_{0.90}O₃ (BCZT) lead-free ceramics demonstrated excellent dielectric, ferroelectric, and piezoelectric properties at the morphotropic phase boundary (MPB). So far, to study the effect of morphological changes on dielectric and ferroelectric properties in lead-free BCZT ceramics, researchers have mostly focused on the influence of spherical grain shape change. In this study, BCZT ceramics with rod-like grains and aspect ratio of about 10 were synthesized by surfactant-assisted solvothermal route. X-ray diffraction (XRD) and selected area electron diffraction (SAED) performed at room temperature confirm the crystallization of pure perovskite with tetragonal symmetry. Scanning electron microscopy (SEM) image showed that BCZT ceramics have kept the 1D rod-like grains with an average aspect ratio of about 4. Rod-like BCZT ceramics exhibit enhanced dielectric ferroelectric ($\epsilon_r = 11,906$, $\tan\delta = 0.014$, $P_r = 6.01 \mu\text{C}/\text{cm}^2$, and $E_c = 2.46 \text{ kV}/\text{cm}$), and electrocaloric properties ($\Delta T = 0.492 \text{ K}$ and $\zeta = 0.289 \text{ (K}\cdot\text{mm)/kV}$ at $17 \text{ kV}/\text{cm}$) with respect to spherical BCZT ceramics. Therefore, rod-like BCZT lead-free ceramics have good potential to be used in solid-state refrigeration technology.

Keywords: lead-free Ba_{0.85}Ca_{0.15}Zr_{0.10}Ti_{0.90}O₃ (BCZT); rod-like Ba_{0.85}Ca_{0.15}Zr_{0.10}Ti_{0.90}O₃ (BCZT); dielectric; ferroelectric; electrocaloric effect

1 Introduction

Due to the constant expansion of industry, increasing

living standard, and climate change, the refrigeration market has become an increasingly significant factor in energy consumption [1–3]. The extensive use of refrigeration is one of the major factors of excessive energy consumption leading to the exhaustion of non-renewable energy resources, and thus deepening

* Corresponding author.

E-mail: m.amjoud@uca.ac.ma

the greenhouse effect. Hence, developing sustainable technological solutions based on promising new cooling technologies is getting increasingly important in recent years. Several efficient techniques are under development such as solar [4], thermoelectric [5], magnetocaloric [6], and electrocaloric cooling [7]. The electrocaloric effect (ECE) has recently shown great potential, as the high electric fields required for the refrigeration cycle are easier and less expensive to produce than the other fields required in competitive refrigeration techniques [8,9]. Giant electrocaloric effect was found in lead-based ferroelectric ceramics like $\text{Pb}(\text{Zr},\text{Ti})\text{O}_3$ (PZT) and $\text{Pb}(\text{Zr},\text{Sn},\text{Ti})\text{O}_3$, as well as in relaxors such as $\text{Pb}(\text{Sc},\text{Nb})\text{O}_3$ and $\text{Pb}(\text{Mg}_{1/3}\text{Nb}_{2/3})\text{O}_3$ – PbTiO_3 (PMN–PT) [10–13]. However, the possible toxicity of lead-based materials limits their application in future eco-friendly cooling systems [3]. Correspondingly, new lead-free materials were developed recently to mimic the properties of lead-based materials [14–16].

Barium titanate (BaTiO_3) is usually regarded as one of potentially promising lead-free ceramics, which was the first material used to fabricate piezoelectric ceramics. It is widely employed in modern technologies such as mobile electronic devices and hybrid electrical vehicles [17,18]. Furthermore, BaTiO_3 is a bioceramic material without any toxic or volatile elements, and its properties can be easily tailored by site engineering [14,19]. However, BaTiO_3 exhibits low dielectric properties compared to lead-based materials and its dielectric constant below the Curie temperature ($T_c = 393$ K) rapidly drops due to the tetragonal/cubic phase transition [20,21]. To overcome the drawback, the $\text{Ba}_{1-x}\text{Ca}_x\text{Zr}_y\text{Ti}_{1-y}\text{O}_3$ system is engineered by introducing Ca^{2+} and Zr^{4+} into the crystal lattice of BaTiO_3 , to replace Ba^{2+} and Ti^{4+} , respectively, with improved dielectric properties due to enhanced relaxor behavior of $\text{Ba}_{1-x}\text{Ca}_x\text{Zr}_y\text{Ti}_{1-y}\text{O}_3$ ceramics [22–26]. Moreover, as reported by Liu and Ren [27], $\text{Ba}_{0.85}\text{Ca}_{0.15}\text{Zr}_{0.10}\text{Ti}_{0.90}\text{O}_3$ (BCZT) phase exhibits interesting dielectric, ferroelectric, and piezoelectric properties at the morphotropic phase boundary (MPB), which is comparable to those of PZT ceramics [15].

It is well known that the electrical properties of any material are very sensitive to its morphology. Almost all published articles on BCZT ceramics studied the dielectric and ferroelectric properties of spherical-grain-based powder [28–30]. Hence, to correlate the electrical and morphological properties, researchers are focusing especially on spherical grain size effect. We

reported previously, the effect of grain size and grain size distribution in BCZT ceramics using surfactant-assisted solvothermal processing [31]. We found that the nature of surfactant directly influences the grain size and grain size distribution of BCZT ceramics. The use of sodium dodecyl sulfate (SDS, $\text{NaC}_{12}\text{H}_{25}\text{SO}_4$) as surfactant results in highly dense ceramics with homogeneous grain distribution. However, cetyltrimethylammonium bromide (CTAB, $\text{C}_{19}\text{H}_{42}\text{BrN}$) surfactant produces BCZT ceramics with bimodal grain size distribution including coarse grains and small spherical ones.

The surfactant-assisted solvothermal synthesis provides a design of nanomaterials with specifically tailored architectures via the synthesis of nanoscale building blocks with an appropriate size and shape, and controlled orientation of the final products. Moreover, the cationic surfactant CTAB, a templating micelle molecule, is used to adjust size and morphology of nanomaterials [32–35]. At the best of our knowledge, there have been no other reports on the electrical studies in rod-like BCZT ceramics. In this contribution, we report the first BCZT ceramics with rod-like grains and evaluate its dielectric, ferroelectric, and electrocaloric properties.

2 Experimental

2.1 Rod-like BCZT powder synthesis

BCZT pure nanocrystalline powder was obtained by CTAB-assisted solvothermal synthesis as reported previously by Ref. [31]. First, an appropriate amount of barium acetate was dissolved in glacial acetic acid. Calcium nitrate tetrahydrate and zirconyl chloride octahydrate were dissolved each alone in 2-methoxyethanol. Second, the three solutions were mixed in a two-neck round bottom flask. In the third stage, titanium^(IV) isopropoxide ($\text{Ti}(\text{O}^i\text{Pr})_4$) was added synchronously dropwise to the reaction medium using an isobaric dropping funnel.

Unlike the previously Ref. [31], to control BCZT microstructure, a different concentration (30 mM) of CTAB surfactant was introduced. The obtained solution was transferred to a 30 mL teflon-lined stainless-steel autoclave at 180 °C in an oven for 12 h. After the reaction was completed, the sealed autoclave was cooled in the air. The resulting product was washed sequentially with ethanol for several times. Then, the final product was dried at 100 °C for 12 h, calcined at

1000 °C for 4 h. Finally, BCZT powder was uniaxially pressed into pellets of diameter of about 6 mm and thickness of about 1 mm, and sintered at 1250 °C/10 h for electrical measurements. For P – E loop measurements, the thickness of the sample was reduced to 0.4 mm to allow high electric field application, while the electrode area was kept to 28.26 mm².

2.2 Characterization rod-like BCZT

The morphology of BCZT powder was investigated by a field-emission scanning electron microscope (FE-SEM, JEOL JSM-7600F). Crystalline structure of BCZT powder was performed by X-ray diffraction (XRD, Panalytical X-Pert Pro). The measurement has been done at room temperature employing a step angle of 0.017° in the 2θ range from 10° to 80° using a Cu K α radiation ($\lambda \approx 1.540598$ Å). The selected area of electronic diffraction (SAED) pattern was recorded by using a transmission electron microscope (TEM, Philips CM200). To determine the optimal calcination temperature of raw BCZT material in order to produce highly pure BCZT powder, the combined thermogravimetric and differential thermal analyses (TG-DTA, Sytram LABSYS evo) were performed at heating rate of 10 °C/min from room temperature to 1100 °C in air. The resulting microstructure of BCZT sintered ceramics was analyzed by using a scanning electron microscope (SEM, Tescan VEGA3). The density of the sintered ceramics was measured by Archimedes method using deionized water as medium. A precision LCR meter (HP 4284A, 20 Hz to 1 MHz) was used to measure the dielectric properties of BCZT ceramic pellet that was electroded with silver paste in the frequency range of 100 Hz–1 MHz. The ferroelectric hysteresis loops were determined by using a ferroelectric test system (AiXACCT, TF Analyzer 3000) at a driving frequency of 1 Hz.

3 Results and discussion

3.1 Thermal analysis and phase evolution

The typical thermal decomposition behavior of the BCZT raw material is shown in Fig. 1. The first weight loss at temperatures between 40 and 160 °C is due to desorption of physically adsorbed water (dehydration phenomena). The second weight loss in the range of 160–230 °C can be attributed to the chemisorbed

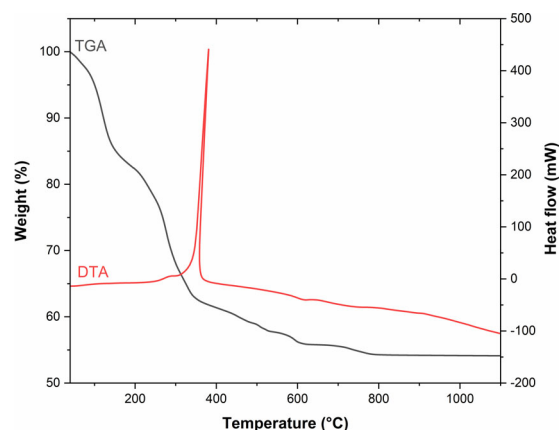


Fig. 1 TG-DTA curves of BCZT raw material.

water (dehydroxylation phenomena). The exothermic located peak at 380 °C is associated to the thermal decomposition of various organic compounds. The fourth loss between 580 and 800 °C is attributed to the formation and crystallization of BCZT phase [36]. Finally, the mass loss remains constant after 800 °C. Based on these analyses, the temperature of 1000 °C was selected as the calcination temperature for the formation of highly pure perovskite BCZT.

3.2 Morphology and phase characterization of rod-like BCZT powder

In Fig. 2(a), a FE-SEM micrograph of the elaborated BCZT powder is presented. Besides very small amount of BCZT nanoparticles that were not yet transformed into BCZT rods, mainly rod-like grains with an average diameter and length of 0.45 and 4.25 μm, respectively, are visible with the corresponding aspect ratio around 10.

The XRD pattern obtained for BCZT calcined powder is shown in Fig. 2(b). It was observed that BCZT powder was formed in a pure perovskite phase, without any trace of crystalline impurities. All diffraction peaks can be indexed based on the standard model X-ray polycrystalline tetragonal BaTiO₃ (JCPDS card No. 96-901-4669) with the space group $P4mm$. The characteristic tetragonal reflection (110) was observed at $2\theta = 31.65^\circ$. BCZT powder has a tetragonal symmetry demonstrated by the peaks (002) and (200) splitting [37–40]. Insets of Fig. 2 clearly illustrate the splitting of these peaks in the 2θ range of 44°–46°. Figure 2(c) depicts SAED patterns of BCZT calcined powder. The d -spacings calculated from the measured ring diameters (i.e., 2.834, 2.313, 1.999, and 1.634 Å), correspond to (110), (111), (002), and (211) planes, respectively. These results are in good agreement with those obtained by XRD.

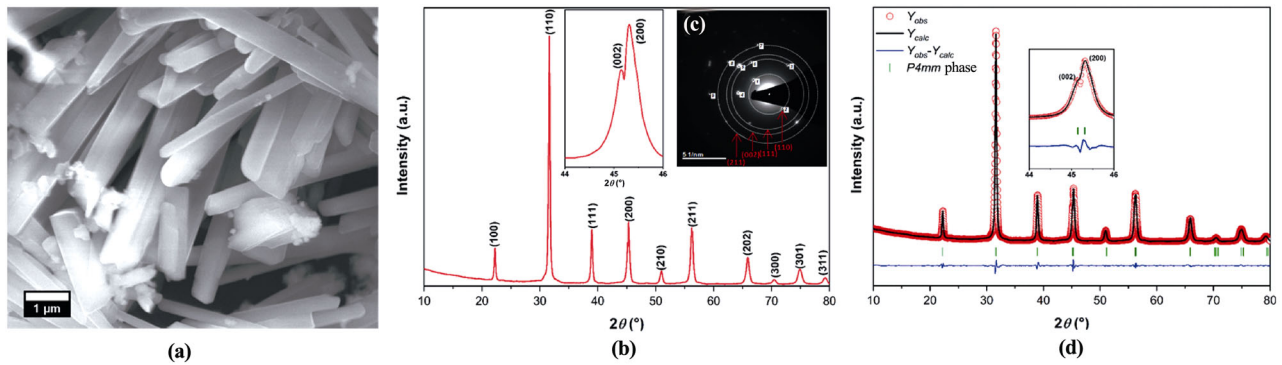


Fig. 2 (a) FE-SEM micrograph, (b) XRD, (c) SAED patterns, and (d) Rietveld refinement of BCZT powder calcined at 1000 °C/4 h.

Phase analysis of BCZT calcined powder was performed in the light of *P4mm* space group as shown in Fig. 2(d). The refinement performed by FullProf Suite software indicates that the diffraction data of BCZT powder collected at room temperature mainly has a tetragonal phase (*P4mm*). Y_{obs} and Y_{calc} correspond to the observed and calculated data respectively. In the Rietveld refinements, Ba and Ca ions are supposed to share the same crystallographic A-site of the BCZT perovskite structure. Similarly, Ti and Zr ions are positioned at the same B-site [40]. Table 1 indicates the lattice parameters, atomic positions, and space group obtained after refinement. These parameters are comparable to those reported in Refs. [40,41].

The degree of tetragonality (c/a) at room temperature

of BCZT is 1.0050. This value is in a good agreement with those of Liu and Ren [27] and Praveen *et al.* [40] which are 1.0050 and 1.0049, respectively.

3.3 Density measurements of rod-like BCZT ceramic

Figure 3 displays SEM micrograph and the corresponding statistical distribution of length and diameter of BCZT ceramics sintered at 1250 °C/10 h. The microstructure reveals tightly bonded and well-defined rod-like grains with no obvious porosity, corresponding to a high bulk density of 5.50 g/cm³ (95% of the theoretical density). The average length and diameter of the rod-like grains are 5.2 and 1.35 μm, respectively. Hence, an average aspect ratio is of 4.

Table 1 Structural parameters obtained from Rietveld refinement of BCZT calcined powder

Lattice parameter (Å)	Angle (°)	Volume (Å ³)		Atomic position (x, y, z)			χ^2	Space group	c/a
$a = 3.99420$	$\alpha = \beta = \gamma = 90$	64.039	Ba/Ca	0.00000	0.00000	0.01674	1.72	<i>P4mm</i>	1.0050
$b = 3.99420$			Zr/Ti	0.50000	0.50000	0.49641			
$c = 4.01410$			O ₁	0.50000	0.50000	-0.03807			
			O ₂	0.50000	0.00000	0.55951			

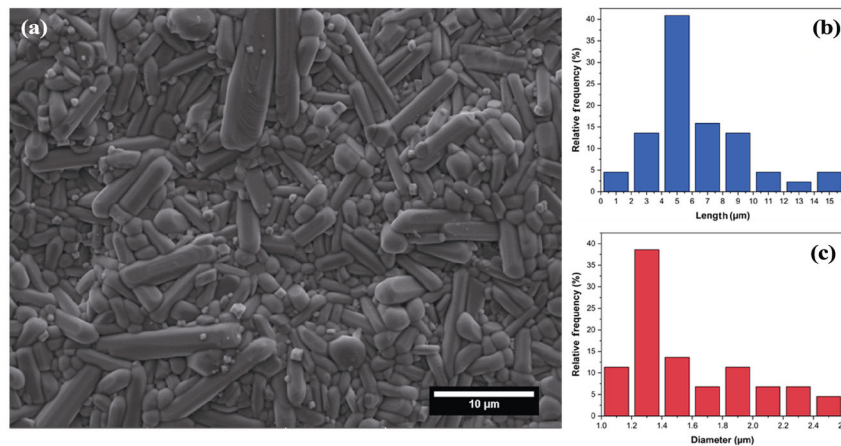


Fig. 3 (a) SEM micrograph and corresponding statistical distribution of (b) length and (c) diameter of BCZT ceramics sintered at 1250 °C/10 h.

3.4 Dielectric and ferroelectric properties of rod-like BCZT ceramics

Figure 4(a) displays the temperature-dependence of the dielectric constant (ϵ_r) and the dielectric loss ($\tan\delta$) of rod-like BCZT ceramics at various frequencies from room temperature to 473 K. The dielectric constant increases with increasing temperature and reaches the maximum at Curie temperature (T_c). A broad anomaly at 366 K associated to the tetragonal–cubic ($T-C$) phase transition was observed [31,42,43]. The broad maximum observed is due to the overlap of several ferroelectric and non-ferroelectric regions [44]. Furthermore, with increasing frequency, the maximum dielectric constant decreases and Curie temperature shifts toward higher temperatures, indicating a typical relaxor frequency dispersion [45,46].

The dielectric constant of normal ferroelectrics above T_c follows the Curie–Weiss law, as described by Eq. (1). The reciprocal dielectric constant was plotted as a function of temperature (T) at 1 kHz and fitted using Curie–Weiss law to evaluate this phase transition:

$$\frac{1}{\epsilon_r} = \frac{T - T_0}{C} \quad (T > T_0) \quad (1)$$

where ϵ_r is the real part of dielectric constant, T_0 is the Curie–Weiss temperature, and C is the Curie–Weiss constant.

The plot of the inverse dielectric constant vs. temperature at 1 kHz is shown in Fig. 4(b). The fitting results obtained by Eq. (1) are listed in Table 2. It was found that the real part of ϵ_r of BCZT ceramics deviates from the Curie–Weiss law above the Curie temperature. The deviations ΔT_m as defined by Eq. (2):

$$\Delta T_m = T_{cw} - T_m \quad (2)$$

where T_{cw} refers to the temperature from which ϵ_r starts to follow the Curie–Weiss law, and T_m denotes the temperature at which ϵ_r value reaches the maximum. The estimated value of deviations ΔT_m is 47 K.

To further confirm the degree of diffuseness in the BCZT ceramics, a modified empirical expression proposed by Uchino and Nomura [47] is used, which is given in Eq. (3):

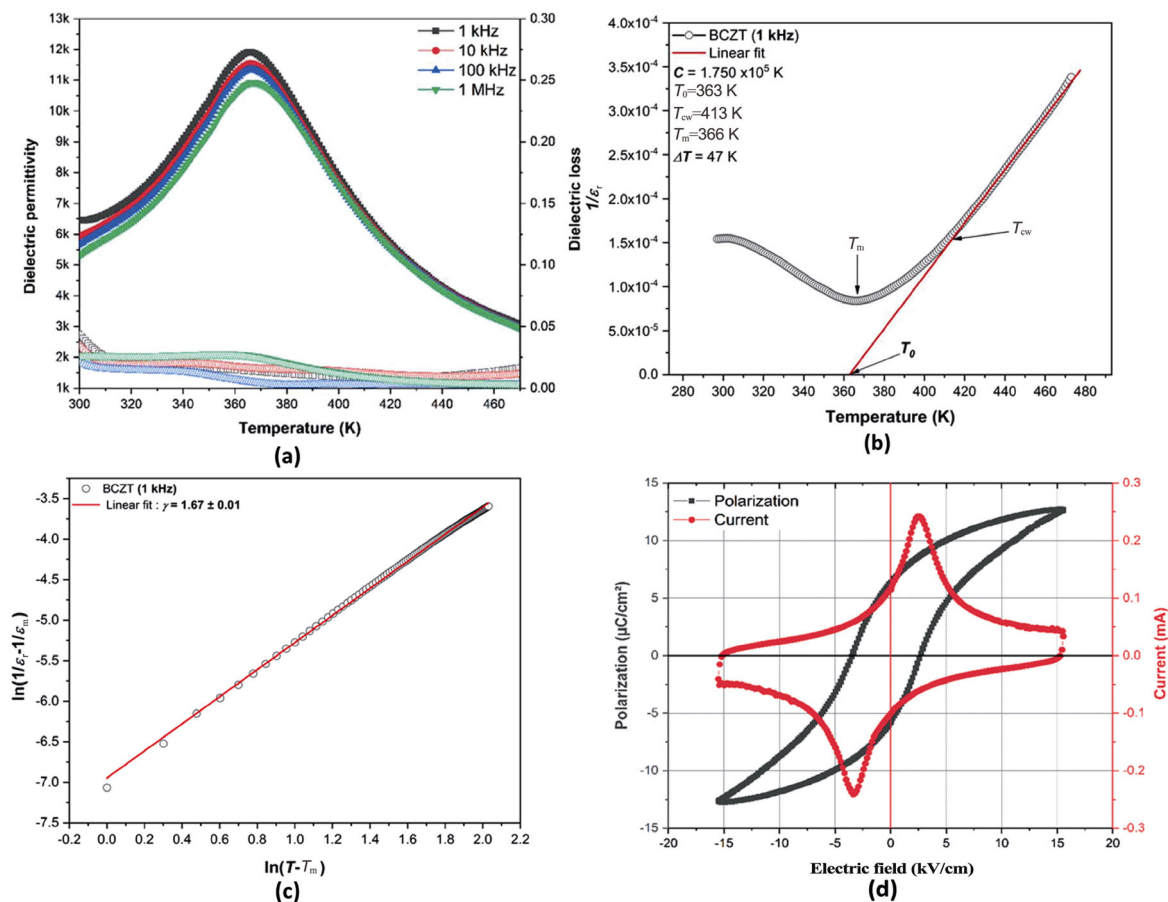


Fig. 4 (a) Temperature-dependence of dielectric constant and dielectric loss, (b, c) plots of Curie–Weiss relation and modified Curie–Weiss law to determine slope (γ), and (d) $P-E$ and $I-E$ plots of BCZT ceramics.

$$\frac{1}{\epsilon_r} - \frac{1}{\epsilon_m} = \frac{(T - T_0)^\gamma}{C} \quad (1 < \gamma < 2) \quad (3)$$

where ϵ_r and ϵ_m are the real part of the dielectric constant and its maximum value, respectively, and γ (degree of diffuse transitions) and C are constants. For an ideal relaxor ferroelectric $\gamma = 2$, while for a normal ferroelectric $\gamma = 1$ and the system follows the Curie–Weiss law [48].

Figure 4(c) depicts the linear fitting plot of $\ln(1/\epsilon_r - 1/\epsilon_m)$ vs. $\ln(T - T_m)$ at 1 kHz for BCZT ceramics. After curve fitting by using Eq. (3), the value obtained for γ at 1 kHz in BCZT ceramics is 1.67.

Previously, we reported the synthesis of BCZT ceramics using CTAB surfactant at different concentrations [31]. It was found that the small spheroidal grains (60–1000 nm) were distributed at the boundaries of coarse grains and occupied the pores created during the sintering to create high dense ceramics with a relative density (D_r) of about 95.2% equal to that of BCZT ceramics with rod-like grains. The dielectric constant and the dielectric loss of BCZT ceramics with spherical grains were found to be 7584 and 0.0158, respectively (Table 2). However, the dielectric constant and the dielectric loss in BCZT ceramics with rod-like grains reached 11,906 and 0.014, respectively. Hence, tailoring BCZT ceramics with large aspect ratio could enhance its dielectric properties [49,50].

P – E and I – E plots of BCZT ceramics at room temperature are represented in Fig. 4(d). It displays a

slim P – E hysteresis loop with remnant polarization (P_r) of 6.01 $\mu\text{C}/\text{cm}^2$ and coercive field (E_c) of 2.46 kV/cm. The I – E curve shows two distinct peaks around the coercive fields, indicating the domain switching phenomena [51]. The appearance of a domain switching current peak (Fig. 4(d)), with an application of electric field confirms the ferroelectric nature of BCZT ceramics. The E_c can be evaluated from the polarization vs. electric field (P – E) hysteresis loop or by the current vs. electric field (I – E) curve [52].

3.5 Electrocaloric effect in rod-like BCZT ceramics

To evaluate the effect of grain shape tailoring on the electrocaloric effect (ECE) in the rod-like BCZT ceramics, Fig. 5(a) depicts P – E hysteresis loops registered at different temperatures at the driving frequency of 1 Hz, as in our recent paper Ref. [25]. The same frequency (1 Hz) was kept to avoid any influence of the frequency as reported by Cheng *et al.* [53]. With increasing the temperature, the remnant polarization decreases continuously due to the disappearance of ferroelectric domains [54].

After recording P – E hysteresis loops as a function of the temperature, we perform a seven-order polynomial fitting by considering only the upper branches of these curves (Fig. 5(a)). Then, the variation of the polarization vs. the temperature at every fixed applied electric field can be deduced (Fig. 5(b)). It was noticed that the polarization decreases slowly from room temperature, then drops rapidly with the temperature around T_c .

Table 2 Dielectric properties of BCZT ceramics with rod-like and spherical-like grains

	ϵ_{max}	$\tan\delta$	D_r (%)	T_0 (K)	C (10^5 K)	T_m (K)	T_{cw} (K)	ΔT_m (K)	γ	Ref.
BCZT rod-like	11,906	0.014	95	363	1.75	366	413	47	1.67	This study
BCZT sphere-like	7584	0.0158	95.2	373	1.812	364	418	54	1.79	[31]

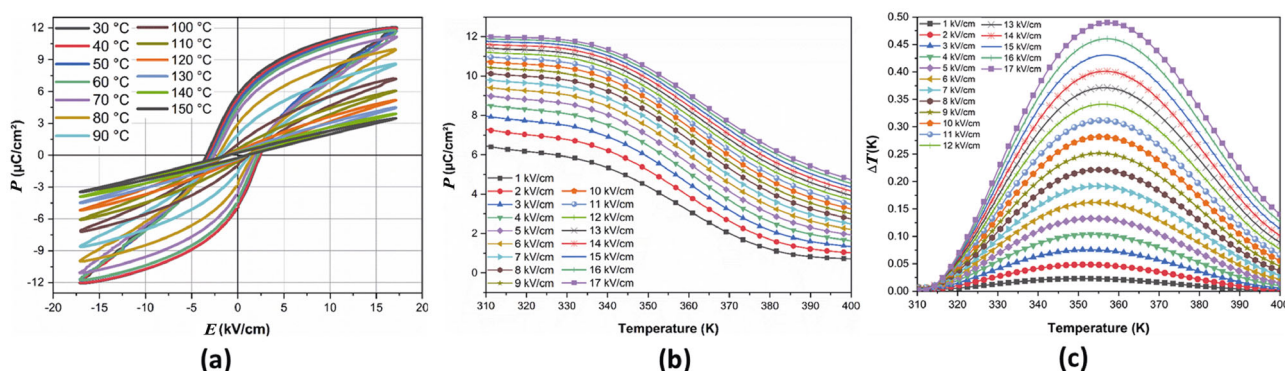


Fig. 5 Temperature-dependence of (a) P – E loops, (b) electric polarization, and (c) the reversible adiabatic electrocaloric temperature change (ΔT) of rod-like BCZT ceramics under various applied electric fields.

ΔT was calculated by indirect method based on Maxwell equation that leads to Eq. (4).

$$\Delta T = - \int_{E_1}^{E_2} \frac{T}{\rho C_p} \left(\frac{\partial P}{\partial T} \right)_E dE \quad (4)$$

where ρ and C_p are the mass density and the specific heat of the material, respectively. The value of C_p (0.378 J/(g·K)) was taken from Ref. [26].

Figure 5(c) shows the temperature-dependence of ΔT . Each curve corresponds to a fixed applied electric field and evidences the ferroelectric–paraelectric phase transition with temperature increasing. The highest value obtained for ΔT was 0.492 K at 17 kV/cm at the tetragonal–cubic transition around 360 K. It is worth noting that a further increase in the applied external electric field could enhance the ΔT value of the material since the P – E loops have not reached saturation yet. Commonly, the electrocaloric responsivity ($\zeta = \Delta T/\Delta E$) is used for more suitable evaluation of the electrocaloric effect of materials. The obtained ΔT value at 17 kV/cm corresponds to the electrocaloric responsivity of $\zeta = 0.289$ (K·mm)/kV.

Our findings are compared with previously published results on BCZT ceramics in Table 3 in which the electrocaloric properties (ΔT and ζ) of BCZT lead-free ceramics with different compositions and shapes are listed. It should be pointed out that ΔT value in the studied rod-like BCZT ceramics was found larger than other reported values in literature [22,37]. However, its electrocaloric responsivity is among the average values. This can be attributed to the elaboration method, the chemical composition, atomic rate, and site occupancy in the structure. It is well known that the nature of the precursors used for the syntheses often plays a key role

in determining the shape and size of the nanomaterials. The nucleation and growth of BCZT from the molecular, ionic, or oxide titanium/zirconium precursors in the presence of barium/calcium carbonates or salts are often dictated by the nature of the cubic crystal structure, which results in the formation of BCZT nanocrystals with spherical or cubic shapes with aspect ratio of about 1 [55]. However, in this study, the CTAB surfactant was used as directing agent to produce BCZT ceramics with rod-like grains.

The ECE is associated with the polarization, phenomenological coefficient, multiple polar states, as well as the breakdown electric field, etc. [56–59]. Indeed, these physical properties are strongly dependent on features and morphologies of dielectric materials such as grain size, size distribution, and aspect ratio. As reported by Zhang *et al.* [60], the electrocaloric properties in Ba_{0.67}Sr_{0.33}TiO₃/Poly (vinylidene fluoride-trifluoroethylene-ter-chlorofluoroethylene) (BST/P (VDF-TrFE-CFE)) nanocomposites by embedding BST fillers with nanoparticles, cubes, rods, and nanowires in morphology are closely related to the aspect ratio of the ceramic BST nanofillers [60]. They found that fillers with high aspect ratio exhibit much higher breakdown and greater ECE. Likewise, Tang *et al.* [49] demonstrated that using high-aspect-ratio of BaTiO₃ (BT) nanowires is an effective way to control and improve the dielectric performance of (BT/PVDF) nanocomposites. Analogically, the enhanced electrocaloric effect in our sample could be attributed to high aspect ratio (4) of BCZT rod-like ceramics as compared with other reported BCZT samples exhibiting almost spherical grains (aspect ratio ≈ 1). Thus, BCZT ceramics with rod-like grains have good potential to be used for the application in eco-friendly solid-state cooling devices.

Table 3 Comparison of the electrocaloric properties of rod-like BCZT ceramics with other lead-free BCZT ceramics reported in literature

Ceramic	ΔT (K)	ΔE (kV/cm)	T (K)	ζ ((K·mm)/kV)	Ref.
Ba _{0.85} Ca _{0.15} Zr _{0.10} Ti _{0.90} O ₃	0.492	17	360	0.289	This study
Ba _{0.85} Ca _{0.15} Zr _{0.10} Ti _{0.90} O ₃	0.118	6.65	363	0.164	[25]
Ba _{0.85} Ca _{0.15} Zr _{0.10} Ti _{0.90} O ₃	0.4	21.5	370	0.186	[37]
Ba _{0.85} Ca _{0.15} Zr _{0.10} Ti _{0.90} O ₃	0.152	8	373	0.19	[26]
Ba _{0.80} Ca _{0.2} Zr _{0.04} Ti _{0.96} O ₃	0.27	7.95	386	0.340	[22]
Ba _{0.80} Ca _{0.20} Zr _{0.08} Ti _{0.92} O ₃	0.22	7.95	386	0.27	[61]
Ba _{0.91} Ca _{0.09} Zr _{0.14} Ti _{0.86} O ₃	0.3	20	328	0.150	[62]
Ba _{0.92} Ca _{0.08} Zr _{0.05} Ti _{0.95} O ₃	0.38	15	410	0.253	[61]

4 Conclusions

In this study, lead-free rod-like BCZT ceramics have been successfully prepared by CTAB-assisted solvothermal processing. XRD and SAED revealed that rod-like BCZT ceramics exhibit pure perovskite phase with tetragonal symmetry and a remarkable c/a of 1.0050 and a high density (95%). SEM micrograph depicted that BCZT ceramics are self-assembled into rod-like grain with an average length and diameter of 5.2 and 1.35 μm , respectively, and therefore with an aspect ratio of 4. Rod-like BCZT ceramics demonstrated

enhanced dielectric ($\epsilon_r = 11,906$, $\tan\delta = 0.014$) and ferroelectric ($P_r = 6.01 \mu\text{C}/\text{cm}^2$ and $E_c = 2.46 \text{ kV}/\text{cm}$) properties compared to BCZT ceramics with spherical grains. Likewise, around 360 K, ΔT and responsivity ζ were found to be 0.492 K and 0.289 (K·mm)/kV, respectively, which are larger than those found in the reported BCZT ceramics. Therefore, lead-free BCZT ceramics with high aspect ratio could be a potential candidate for cooling material in novel environmentally friendly solid-state cooling devices.

Acknowledgements

The authors gratefully acknowledge the generous financial support of CNRST Priority Program (PPR 15/2015), Slovenian Research Agency Program (P1-0125), and European Union's Horizon 2020 Research and Innovation Program under the Marie Skłodowska-Curie Grant Agreement (No. 778072).

References

- [1] Kitanovski A, Plaznik U, Tomc U, *et al.* Present and future caloric refrigeration and heat-pump technologies. *Int J Refrig* 2015, **57**: 288–298.
- [2] Suchanek G, Pakhomov O, Gerlach G. Electrocaloric cooling. In *Refrigeration*. Orhan E, Ed. InTechOpen, 2017.
- [3] Mathur ND. Future trends in electrocalorics materials. In *Electrocaloric Materials*. Correia T, Zhang Q, Eds. Berlin, Heidelberg: Springer Berlin Heidelberg, 2013: 251–253.
- [4] Zhang J, Xuan YM. An integrated design of the photovoltaic-thermoelectric hybrid system. *Sol Energy* 2019, **177**: 293–298.
- [5] Lu X, Zhao DL, Ma T, *et al.* Thermal resistance matching for thermoelectric cooling systems. *Energy Convers Manag* 2018, **169**: 186–193.
- [6] Taboada-Moreno CA, Sánchez-De Jesús F, Pedro-García F, *et al.* Large magnetocaloric effect near to room temperature in Sr doped $\text{La}_{0.7}\text{Ca}_{0.3}\text{MnO}_3$. *J Magn Magn Mater* 2020, **496**: 165887.
- [7] Du HL, Chang YF, Li CW, *et al.* Ultrahigh room temperature electrocaloric response in lead-free bulk ceramics via tape casting. *J Mater Chem C* 2019, **7**: 6860–6866.
- [8] Ožbolt M, Kitanovski A, Tušek J, *et al.* Electrocaloric vs. magnetocaloric energy conversion. *Int J Refrig* 2014, **37**: 16–27.
- [9] Quintero M, Ghivelder L, Gomez-Marlasca F, *et al.* Decoupling electrocaloric effect from Joule heating in a solid state cooling device. *Appl Phys Lett* 2011, **99**: 232908.
- [10] Kutnjak Z, Rožič B, Pirc R. Wiley Encyclopedia of Electrical and Electronics Engineering. In *Electrocaloric Effect: Theory, Measurements, and Applications*. Hoboken, NJ, USA: John Wiley & Sons, Inc., 2015: 1–19.
- [11] Tuttle BA, Payne DA. The effects of microstructure on the electrocaloric properties of $\text{Pb}(\text{Zr},\text{Sn},\text{Ti})\text{O}_3$ ceramics. *Ferroelectrics* 1981, **37**: 603–606.
- [12] Qiu JH, Jiang Q. Effect of electric field on electrocaloric effect in $\text{Pb}(\text{Zr}_{1-x}\text{Ti}_x)\text{O}_3$ solid solution. *Phys Lett A* 2008, **372**: 7191–7195.
- [13] Xiao D, Wang Y, Zhang R, *et al.* Electrocaloric properties of $(1-x)\text{Pb}(\text{Mg}_{1/3}\text{Nb}_{2/3})\text{O}_{3-x}\text{PbTiO}_3$ ferroelectric ceramics near room temperature. *Mater Chem Phys* 1998, **57**: 182–185.
- [14] Gao JH, Xue DZ, Liu WF, *et al.* Recent progress on BaTiO_3 -based piezoelectric ceramics for actuator applications. *Actuators* 2017, **6**: 24.
- [15] Panda PK, Sahoo B. PZT to lead free piezo ceramics: A review. *Ferroelectrics* 2015, **474**: 128–143.
- [16] Rödel J, Jo W, Seifert KTP, *et al.* Perspective on the development of lead-free piezoceramics. *J Am Ceram Soc* 2009, **92**: 1153–1177.
- [17] Puli VS, Pradhan DK, Chrisey DB, *et al.* Structure, dielectric, ferroelectric, and energy density properties of $(1-x)\text{BZT}-x\text{BCT}$ ceramic capacitors for energy storage applications. *J Mater Sci* 2013, **48**: 2151–2157.
- [18] Hu PH, Shen Y, Guan YH, *et al.* Topological-structure modulated polymer nanocomposites exhibiting highly enhanced dielectric strength and energy density. *Adv Funct Mater* 2014, **24**: 3172–3178.
- [19] Coondoo I, Panwar N, Amorín H, *et al.* Synthesis and characterization of lead-free $0.5\text{Ba}(\text{Zr}_{0.2}\text{Ti}_{0.8})\text{O}_3-0.5(\text{Ba}_{0.7}\text{Ca}_{0.3})\text{TiO}_3$ ceramic. *J Appl Phys* 2013, **113**: 214107.
- [20] Wang FJ, Li W, Jiang HL, *et al.* Preparation and dielectric properties of $\text{Ba}_{0.95}\text{Ca}_{0.05}\text{Ti}_{0.8}\text{Zr}_{0.2}\text{O}_3$ -polyethersulfone composites. *J Appl Phys* 2010, **107**: 043528.
- [21] Liu X, Wu D, Chen Z, *et al.* Ferroelectric, dielectric and pyroelectric properties of Sr and Sn codoped BCZT lead free ceramics. *Adv Appl Ceram* 2015, **114**: 436–441.
- [22] Asbani B, Dellis JL, Lahmar A, *et al.* Lead-free $\text{Ba}_{0.8}\text{Ca}_{0.2}(\text{Zr}_x\text{Ti}_{1-x})\text{O}_3$ ceramics with large electrocaloric effect. *Appl Phys Lett* 2015, **106**: 042902.
- [23] Luo BC, Wang XH, Wang YP, *et al.* Fabrication, characterization, properties and theoretical analysis of ceramic/PVDF composite flexible films with high dielectric constant and low dielectric loss. *J Mater Chem A* 2014, **2**: 510–519.
- [24] Hanani Z, Ablouh EH, Amjoud M', *et al.* Very-low temperature synthesis of pure and crystalline lead-free $\text{B}_{0.85}\text{C}_{0.15}\text{Zr}_{0.1}\text{Ti}_{0.9}\text{O}_3$ ceramic. *Ceram Int* 2018, **44**: 10997–11000.
- [25] Hanani Z, Mezzane D, Amjoud M, *et al.* Phase transitions, energy storage performances and electrocaloric effect of the lead-free $\text{Ba}_{0.85}\text{Ca}_{0.15}\text{Zr}_{0.1}\text{Ti}_{0.9}\text{O}_3$ ceramic relaxor. *J Mater Sci: Mater Electron* 2019, **30**: 6430–6438.
- [26] Kaddoussi H, Lahmar A, Gagou Y, *et al.* Sequence of structural transitions and electrocaloric properties in $(\text{Ba}_{1-x}\text{Ca}_x)(\text{Zr}_{0.1}\text{Ti}_{0.9})\text{O}_3$ ceramics. *J Alloys Compd* 2017,

- 713: 164–179.
- [27] Liu WF, Ren XB. Large piezoelectric effect in Pb-free ceramics. *Phys Rev Lett* 2009, **103**: 257602.
- [28] Bai Y, Matousek A, Tofel P, *et al.* (Ba,Ca)(Zr,Ti)O₃ lead-free piezoelectric ceramics—The critical role of processing on properties. *J Eur Ceram Soc* 2015, **35**: 3445–3456.
- [29] Hao JG, Bai WF, Li W, *et al.* Correlation between the microstructure and electrical properties in high-performance (Ba_{0.85}Ca_{0.15})(Zr_{0.1}Ti_{0.9})O₃ lead-free piezoelectric ceramics. *J Am Ceram Soc* 2012, **95**: 1998–2006.
- [30] Shi J, Lu XY, Shao JH, *et al.* Effects on structure and properties of BCZT lead-free piezoelectric ceramics by rare-earth doping. *Ferroelectrics* 2017, **507**: 186–197.
- [31] Hanani Z, Mezzane D, Amjoud M, *et al.* Enhancement of dielectric properties of lead-free BCZT ferroelectric ceramics by grain size engineering. *Superlattices Microstruct* 2019, **127**: 109–117.
- [32] Zhao PJ, Wang L, Bian L, *et al.* Growth mechanism, modified morphology and optical properties of coral-like BaTiO₃ architecture through CTAB assisted synthesis. *J Mater Sci Technol* 2015, **31**: 223–228.
- [33] Wang YX, Sun J, Fan XY, *et al.* A CTAB-assisted hydrothermal and solvothermal synthesis of ZnO nanopowders. *Ceram Int* 2011, **37**: 3431–3436.
- [34] Yayapao O, Thongtem T, Phuruangrat A, *et al.* CTAB-assisted hydrothermal synthesis of tungsten oxide microflowers. *J Alloys Compd* 2011, **509**: 2294–2299.
- [35] Vijayalakshmi R, Rajendran V. Impact of surfactants on physical properties of BaTiO₃ nanoparticles. *Int J Nanosci* 2013, **12**: 1350003.
- [36] Praveen JP, Karthik T, James AR, *et al.* Effect of poling process on piezoelectric properties of sol–gel derived BZT–BCT ceramics. *J Eur Ceram Soc* 2015, **35**: 1785–1798.
- [37] Patel S, Sharma P, Vaish R. Enhanced electrocaloric effect in Ba_{0.85}Ca_{0.15}Zr_{0.1}Ti_{0.9–x}Sn_xO₃ ferroelectric ceramics. *Phase Transit* 2016, **89**: 1062–1073.
- [38] Roy S, Maharana R, Reddy SR, *et al.* Structural, ferroelectric and piezoelectric properties of chemically processed, low temperature sintered piezoelectric BZT–BCT ceramics. *Mater Res Express* 2016, **3**: 035702.
- [39] Xu HR, Gao L, Guo JK. Preparation and characterizations of tetragonal barium titanate powders by hydrothermal method. *J Eur Ceram Soc* 2002, **22**: 1163–1170.
- [40] Praveen JP, Karthik T, James AR, *et al.* Effect of poling process on piezoelectric properties of sol–gel derived BZT–BCT ceramics. *J Eur Ceram Soc* 2015, **35**: 1785–1798.
- [41] Jeong IK, Ahn JS. The atomic structure of lead-free Ba(Zr_{0.2}Ti_{0.8})O₃–(Ba_{0.7}Ca_{0.3})TiO₃ by using neutron total scattering analysis. *Appl Phys Lett* 2013, **102**: 179903.
- [42] Wang ZM, Wang JJ, Chao XL, *et al.* Synthesis, structure, dielectric, piezoelectric, and energy storage performance of (Ba_{0.85}Ca_{0.15})(Ti_{0.9}Zr_{0.1})O₃ ceramics prepared by different methods. *J Mater Sci: Mater Electron* 2016, **27**: 5047–5058.
- [43] Bai WF, Chen DQ, Zhang JJ, *et al.* Phase transition behavior and enhanced electromechanical properties in (Ba_{0.85}Ca_{0.15})(Zr_xTi_{1–x})O₃ lead-free piezoceramics. *Ceram Int* 2016, **42**: 3598–3608.
- [44] Venkata RE, Mahajan A, Graça MPF, *et al.* Structure and ferroelectric studies of (Ba_{0.85}Ca_{0.15})(Ti_{0.9}Zr_{0.1})O₃ piezoelectric ceramics. *Mater Res Bull* 2013, **48**: 4395–4401.
- [45] Bokov AA, Ye ZG. Recent progress in relaxor ferroelectrics with perovskite structure. In *Frontiers of Ferroelectricity*. Boston, MA: Springer US, 2007: 31–52.
- [46] Liu YW, Pu YP, Sun ZX. Enhanced relaxor ferroelectric behavior of BCZT lead-free ceramics prepared by hydrothermal method. *Mater Lett* 2014, **137**: 128–131.
- [47] Uchino K, Nomura S. Critical exponents of the dielectric constants in diffused-phase-transition crystals. *Ferroelectr Lett Sect* 1982, **44**: 55–61.
- [48] Uchino K. Advanced Piezoelectric Materials. In *Relaxor Ferroelectric-Based Ceramics*. Elsevier, 2017: 127–153.
- [49] Tang HX, Zhou Z, Sodano HA. Relationship between BaTiO₃ nanowire aspect ratio and the dielectric permittivity of nanocomposites. *ACS Appl Mater Interfaces* 2014, **6**: 5450–5455.
- [50] Chary KS, Panda HS, Prasad CD. Fabrication of large aspect ratio Ba_{0.85}Ca_{0.15}Zr_{0.1}Ti_{0.9}O₃ superfine fibers-based flexible nanogenerator device: Synergistic effect on curie temperature, harvested voltage, and power. *Ind Eng Chem Res* 2017, **56**: 10335–10342.
- [51] Kumar A, Bhanu Prasad VV, James Raju KC, *et al.* Optimization of poling parameters of mechanically processed PLZT 8/60/40 ceramics based on dielectric and piezoelectric studies. *Eur Phys J B* 2015, **88**: 287.
- [52] Zhan D, Xu Q, Huang DP, *et al.* Dielectric nonlinearity and electric breakdown behaviors of Ba_{0.95}Ca_{0.05}Zr_{0.3}Ti_{0.7}O₃ ceramics for energy storage utilizations. *J Alloys Compd* 2016, **682**: 594–600.
- [53] Cheng XY, Weyland F, Novak N, *et al.* Indirect electrocaloric evaluation: Influence of polarization hysteresis measurement frequency. *Phys Status Solidi A* 2019, **216**: 1900684.
- [54] Hamza A, Benabdallah F, Kallel I, *et al.* Effect of rare-earth substitution on the electrical properties and Raman spectroscopy of BCTZ ceramics. *J Alloys Compd* 2018, **735**: 2523–2531.
- [55] Chen XF, Chao XL, Yang ZP. Submicron Barium calcium zirconium titanate ceramic for energy storage synthesised via the co-precipitation method. *Mater Res Bull* 2019, **111**: 259–266.
- [56] Lu B, Yao YB, Jian XD, *et al.* Enhancement of the electrocaloric effect over a wide temperature range in PLZT ceramics by doping with Gd³⁺ and Sn⁴⁺ ions. *J Eur Ceram Soc* 2019, **39**: 1093–1102.
- [57] Jian XD, Lu B, Li DD, *et al.* Direct measurement of large electrocaloric effect in Ba(ZrxTi_{1–x})O₃ ceramics. *ACS Appl Mater Interfaces* 2018, **10**: 4801–4807.

- [58] Lu B, Li PL, Tang ZH, *et al.* Large electrocaloric effect in relaxor ferroelectric and antiferroelectric lanthanum doped lead zirconate titanate ceramics. *Sci Rep* 2017, **7**: 45335.
- [59] Li XY, Lu SG, Chen XZ, *et al.* Pyroelectric and electrocaloric materials. *J Mater Chem C* 2013, **1**: 23–37.
- [60] Zhang GZ, Zhang XS, Yang TN, *et al.* Colossal room-temperature electrocaloric effect in ferroelectric polymer nanocomposites using nanostructured Barium strontium titanates. *ACS Nano* 2015, **9**: 7164–7174.
- [61] Singh G, Tiwari VS, Gupta PK. Electro-caloric effect in $(\text{Ba}_{1-x}\text{Ca}_x)(\text{Zr}_{0.05}\text{Ti}_{0.95})\text{O}_3$: A lead-free ferroelectric material. *Appl Phys Lett* 2013, **103**: 202903.
- [62] Bai Y, Han X, Qiao LJ. Optimized electrocaloric refrigeration capacity in lead-free $(1-x)\text{BaZr}_{0.2}\text{Ti}_{0.8}\text{O}_3-x\text{Ba}_{0.7}\text{Ca}_{0.3}\text{TiO}_3$ ceramics. *Appl Phys Lett* 2013, **102**: 252904.

Open Access This article is licensed under a Creative Commons Attribution 4.0 International License, which permits use, sharing, adaptation, distribution and reproduction in any medium or format, as long as you give appropriate credit to the original author(s) and the source, provide a link to the Creative Commons licence, and indicate if changes were made.

The images or other third party material in this article are included in the article's Creative Commons licence, unless indicated otherwise in a credit line to the material. If material is not included in the article's Creative Commons licence and your intended use is not permitted by statutory regulation or exceeds the permitted use, you will need to obtain permission directly from the copyright holder.

To view a copy of this licence, visit <http://creativecommons.org/licenses/by/4.0/>.